Available online at www.sciencedirect.com
SCIENCE DIRECT®
European Journal of Pharmaceutics and Biopharmaceutics 63 (2006) 115–127
European Journal of Pharmaceutics and Biopharmaceutics
www.elsevier.com/locate/ejpb

Research paper

Physical stability, centrifugation tests, and entrapment efficiency studies of carnauba wax–decyl oleate nanoparticles used for the dispersion of inorganic sunscreens in aqueous media

J.R. Villalobos-Hernández, C.C. Müller-Goymann *

Institut für Pharmazeutische Technologie, Technische Universität Braunschweig, Braunschweig, Germany

Received 23 November 2005; accepted in revised form 11 January 2006
Available online 18 April 2006

Abstract

Aqueous nanoscale lipid dispersions consisting of carnauba wax–decyl oleate mixtures acting as carriers or accompanying vehicles for inorganic sunscreens such as barium sulfate, strontium carbonate, and titanium dioxide were prepared by high pressure homogenization. For the manufacture of these nanosuspensions, three pigment concentrations (%wt), namely 2, 4, and 6, and two carnauba wax–decyl oleate ratios, 1:1 and 2:1, were used, being some of these combinations chosen for stability studies. Six-month physical stability tests at 4, 20, and 40 °C selecting the mean particle size and the polydispersity index of the nanosuspensions as reference parameters were performed. Centrifugation tests of the nanosuspensions assessed by transmission electron microscopy and by the determination of the content of pigments and carnauba wax in the separated fractions were done. The mean particle sizes and the polydispersity indices of the nanosuspensions were not altered after six-month storages at 20 and at 40 °C. However, the storage of those at 4 °C considerably increased the particle size and polydispersity of the systems, particularly when wax–oil ratios (2:1) were used for the entrapment of the pigments. Transmission electron micrographs of centrifuged samples denoted the presence of three major fractions showing the different types of particles integrated into the nanosuspensions. Furthermore, it was observed that not all the carnauba wax participated in the entrapment of the pigment. Regarding the amount of pigment being encapsulated or bonded by the wax–oil matrices, entrapment efficiencies higher than 85.52% were reported.

Keywords: Nanosuspensions; Inorganic sunscreens; Physical stability; Centrifugation; Entrapment efficiency; Transmission electron microscopy

1. Introduction

Modifications of solid lipid nanoparticles composed of binary mixtures of solid lipids and liquid lipids recently referred to as nanostructured lipid carriers (NLCs) constitute suitable vehicles for the dermal delivery of different drugs [1]. The original purpose of those mixtures was to avoid lipid re-crystallization causing an expulsion of the enclosed actives [2,3]. However, such combinations have also been found to offer protection against chemical degradation of drugs, to contribute to the solubilization of poorly soluble drugs and particularly, in the case of sunscreens, to enhance the sun protection factor [4–6]. Like any other pharmaceutical or cosmetic product, the performance of a sunscreen must be supported by stability tests to observe the possible changes in the formulation, which is particularly important during preformulatory stages [7]. NLCs, in similar way to other disperse systems, may face stability problems attributed to physical, chemical, and microbiological factors. Consequently, the destabilization of those systems can be reflected by changes in particle size, homogeneity, chemical composition, and growth of microorganisms [8]. To carry out a protocol of long-term

* Corresponding author. Institut für Pharmazeutische Technologie, Technische Universität Braunschweig, Mendelssohnstr. 1, D-38106 Braunschweig, Germany. Tel.: +49 531 3915650; fax: +49 531 3918108.
E-mail address: c.mueller-goymann@tu-bs.de (C.C. Müller-Goymann).

0939-6411/$ - see front matter © 2006 Elsevier B.V. All rights reserved.
doi:10.1016/j.ejpb.2006.01.005

stability on drug products, stress variables are required. In this sense, one of those widely accepted stress factors is the variation of the temperature [9]. This is justified because of the different changes provoked by this factor, i.e., the acceleration of the chemical reactions; the phase separation or aggregation phenomena; the viscosity modification of the phases and the increase of the Brownian movement [10,11]. Thus, through the use of temperature, it is possible to identify the weakness of a formulation; to establish optimal storage conditions and to make stability predictions in some cases [12]. The information generated through stability studies can also be used for reformulation purposes considering properties such as the type of emulsifier and its concentration, the zeta potential of the particles, the thermodynamically most stable particle size, the use of preservatives, and the selection of the primary packaging material [13–15]. On the other hand, in order to judge the suitability of a nanoscale carrier system, besides the stability of the system, the incorporation of the actives into the lipid matrices, defined as loading capacity or entrapment efficiency, has also to be evaluated [16,17]. This parameter can be related to different variables such as the drug/lipid ratio applied, surfactant interactions, and the intrinsic lipid crystallization behavior, the latter being particularly important after long time storage [18–20]. To achieve the evaluation of the loading capacity, centrifugation and ultracentrifugation techniques followed by different analytical methods for the drug determination depending on the lipids and actives used have been proposed for the separation of nanoparticles before [21–23]. Through these techniques, the separation of the different structures contained in nanosuspensions or nanoemulsions along a given centrifugation media can be carried out in terms of their densities [24]. This property could be certainly advantageous not only to quantify the separated species, but also to obtain a better visualization of them, especially when microscopic methods are applied [25]. In a previous work of this group, it was observed that inorganic sunscreens like barium sulfate, strontium carbonate, and titanium dioxide could be successfully incorporated into NLCs and that this association of pigment and lipid matrices was the key to reach high sun protection factors [26]. Meanwhile in vivo tests of those colloidal systems demonstrated not to modify the skin barrier function, particularly when titanium dioxide wax used in combination with wax–oil matrices. Nevertheless, information related to the long-term stability of those systems; the type of particle associations integrated into those nanosuspensions; the distribution of pigment and wax after centrifugation and the entrapment efficiency have not been provided so far. The purpose of this work was to complete these aspects in order to obtain a better characterization of the system, by which, it could be possible to find out the best storage conditions, to suggest changes for the stabilization of the product under adverse conditions, and to evaluate the current entrapment efficiency of the systems. To reach this goal, six-month physical stability tests at three different temperatures, namely 4, 20, and 40 °C, were performed using the mean particle size and the polydispersity index of the nanosuspensions as reference parameters. Centrifugation tests using a saccharose solution 20%wt as separation medium were also done and the obtained fractions were quantified spectrophotometrically in the case of carnauba wax and gravimetrically in that of the pigments. These studies were further completed with the microscopic electronic visualization of the structures located at different positions inside the centrifuged tubes. Finally, the performed research will contribute to improve the distribution of the inorganic sunscreens inside the lipid matrices to rationalize the use of sunscreen formulations in ulterior studies.

2. Materials

Alumina–stearic acid surface-treated nanofine titanium dioxide having a primary particle size (PPS) of about 17 nm (Kemira OY, Finland), nanofine barium sulfate (PPS ca. 30 nm) (Solvay GmbH, Germany), strontium carbonate (PPS ca. 30 nm) (Solvay GmbH, Germany), carnauba wax Ph. Eur. and decyl oleate (Caelo GmbH, Germany), Tween® 80 (Atlas Chemie GmbH, Germany), simethicone antifoamer (Sigma–Aldrich GmbH, Germany), and methylisothiazolinone (Brenntag GmbH, Germany) were used. Bidistilled and filtered water (0.2 μm) was used for each preparation. Biochemical grade saccharose (MERCK KGaA, Germany) was purchased for the centrifugation tests and analytical grade toluene (Sigma–Aldrich GmbH, Germany) was used for the quantification of carnauba wax.

3. Experimental methods

3.1. Manufacture of applied formulations

The chemical compositions of the prepared dispersions and the distribution of the pigments in the different phases, oil phase or aqueous phase, are shown in Table 1.

Table 1
The chemical composition and concentration of the tested formulations

		Formulation		
Substances	wt (%)	I	II	III
Decyl oleate	5	+	+	+
Carnauba wax	5, 10	+	+	+
Pigment*	2, 4, 6	−	+ (LP)	+ (AP)
Tween 80	1	+	+	+
Methylisothiazoline	0.028	+	+	+
Simethicone	0.01	+	+	+
Double dist. water	q.s. 100	+	+	+

Key: (*) = barium sulfate, strontium carbonate or titanium dioxide (−) = absent, (+) = present, LP = lipid phase, AP = aqueous phase, q.s. = quantum sufficient or quantity sufficient to make.
Formulation key: I, nanosuspensions of carnauba wax–decyl oleate matrices; II, nanosuspensions of carnauba wax–decyl oleate matrices loaded with pigments in the lipid phase; III, nanosuspensions of carnauba wax–decyl oleate matrices loaded with titanium dioxide in the aqueous phase.

3.1.1. Nanosuspensions of carnauba wax–decyl oleate matrices (Formulation I)

This formulation was produced by dispersing a lipid phase into an aqueous phase using high pressure homogenization as indicated in Table 1. The phases were initially predispersed during 5 min at a speed of 26,000 rpm by means of an Ultraturrax (IKA, Germany) at a temperature of 90 ± 5 °C and subsequently high pressure homogenized at 300 bar ± 10 bar within 30 passes using an homogenizer Niro Type II (Niro Soavi S.p.A., Italy). This latter process was performed at a temperature of 75 ± 5 °C. After the homogenization, the product was cooled down at room temperature, the loss of water was compensated, and the preservative was added. It has to be pointed out that according to further experiments, similar homogenization results could be obtained within 15 passes at the same temperature and pressure. Moreover, neither a lower number of passes nor the application of a higher pressure using the aforementioned homogenizer can be recommended because they do not contribute to reduce the mean particle size or to improve the polydispersity index of the system. However, since the homogenization parameters strongly depend on the equipment used to carry out this process and the intrinsic properties of the materials to be homogenized as well, similar results could be obtained under other conditions with different homogenizers [27].

3.1.2. Nanosuspensions of carnauba wax–decyl oleate matrices loaded with pigments distributed in the lipid phase (Formulation II)

The lipid phase composed of the inorganic pigment, decyl oleate, and carnauba wax was previously prepared by melting the wax at 90 ± 5 °C and mixing it with the oil and the pigment by means of magnetic stirring during 30 min. This step permitted to eliminate the large clumps of titanium dioxide in order to achieve an homogeneous paste. The aforementioned temperature was kept along this mixing process. Thereafter, the lipid phase was combined with the aqueous phase as described in Section 3.1.1.

3.1.3. Nanosuspensions of carnauba wax–decyl oleate matrices loaded with titanium dioxide distributed in the aqueous phase (Formulation III)

A formula containing freely dispersed titanium dioxide crystals in the presence of lipid nanoparticles was prepared. A carnauba wax–decyl oleate dispersion was made by high pressure homogenization and cooled down to room temperature. Titanium dioxide was added and pre-dispersed by stirring at 26,000 rpm during 5 min using an Ultraturrax (IKA, Germany). The dispersion was high pressure homogenized at 300 bar ± 10 bar within 30 passes at room temperature.

3.2. Photon correlation spectroscopy (PCS) and polydispersity indices (PI)

The particle diameters and polydispersity indices were simultaneously measured by PCS using a Zetasizer 3 (Malvern, Germany) modified with an He/Ne laser model 127 (Spectra Physics, USA). The detection was performed at 90° in a cell AZ 10 equilibrated at 293 K. The samples were diluted with double-filtered distilled water to provide recommended scattering activity. Three samples of each preparation were used and every sample was measured twice.

3.3. Stability tests

Two 3-mL samples from pigment-free carnauba wax–decyl oleate (CW:DO) nanoparticle suspensions at two different ratios (1:1 and 2:1) and from pigment-loaded CW:DO-nanoparticle suspensions at the same wax–oil ratios were evaluated. The pigments used were barium sulfate, strontium carbonate, and titanium dioxide. The pigment loads applied were 2%wt and 6%wt, and they were distributed in the lipid phase and only in the case of titanium dioxide, pigment dispersions in the aqueous phase of the suspension were also prepared. The samples were stored for six months at 4, 20, and 40 °C in conditioned places. In order to avoid interference from other factors such as light and water loss, the samples were placed into 5-mL brown gas chromatographic bottles and sealed with aluminum-ringed butyl/PTFE layered rubber stoppers (VWR Int., Germany). The mean particle size (z-average) and the polydispersity index of the samples were measured after 0, 15, 30, 60, 90, and 180 days.

3.4. Centrifugation

One gram samples of the different nanosuspensions were dispersed in 25 mL of a saccharose solution 20%wt ($\rho = 1.0584$ g/mL) and centrifuged for 1 h at 10,400g at room temperature to obtain two fractions simply identified as supernatant (su) and sediment (se). The equipment used was a centrifuge Allegra™ 64R (Beckman Coulter, USA). The separated fractions were removed for later TEM viewing. The use of a concentrated saccharose solution, like in the case of many biological separations, contributed to maintain the separation amongst the different kinds of nanoparticles because of their different densities at the end of the centrifugation [28]. However, in this case the exact density of the separated nanoparticles was not determined.

3.5. Transmission electron microscopy (TEM)

Samples of the nanosuspensions were first freeze fractured at −100 °C at a pressure of 5×10^{-6} bar in a BAF 400 device was (Balzers, Germany). Thereafter they were shadowed with platinum/carbon (layer thickness 2 nm) at 45° and stabilized with carbon (layer thickness 20 nm) at 90°. Replicas were cleaned with sulfuric acid and viewed with a LEO 120 (Leo Inst., Germany) at 125 kV.

3.6. Determination of pigment content by gravimetry

Two 1-g samples of each nanosuspension were centrifuged as indicated in Section 3.4. The separated fractions were carefully deposited in previously tared porcelain capsules. The excess of water was allowed to evaporate overnight in an oven at a temperature of 85 °C. The samples in capsules were pre-fumed at 300 °C with a heat plate to eliminate the excess of saccharose and subsequently heated at 600 °C during 1 h using a muffle furnace. The capsules containing ashes of the inorganic pigments from the different fractions were weighted and their contents were estimated by weight difference using the weight of the previously tared empty capsules as references. This relationship can be expressed by the following equation

$$PC_f = W_{\text{capsule with pigment in the fraction}} - W_{\text{empty capsule}}, \quad (1)$$

where $PC_f = PC_{su}$ or PC_{se}.

The total content of pigment (PC_t %) could be found by the sum of the pigment content in both fractions, i.e., the pigment content at the supernatant (PC_{su} %) and the pigment content at the sediment (PC_{se} %). The PC_{su} %, PC_{se} %, and PC_t % are given by the following equations:

$$PC_{su}\ \% = \left(\frac{PC_{su}}{PC_{su} + PC_{se}}\right) \times 100, \quad (2)$$

$$PC_{se}\ \% = \left(\frac{PC_{se}}{PC_{su} + PC_{se}}\right) \times 100, \quad (3)$$

$$PC_t\ \% = PC_{su}\ \% + PC_{se}\ \%. \quad (4)$$

3.7. Entrapment efficiency

As described above, the PC_{se} % represents the amount of pigment at the sediment and consists of wax–oil matrices with encapsulated or bonded pigments. Hence, this value can be referred to as the efficiency of entrapment (EE%) in the system according to the following equation

$$PC_{se}\ \% = EE\ \%. \quad (5)$$

However, Eq. (5) is only valid for the case of those formulations prepared from a lipid phase with pigments added to the molten wax. For those nanosuspensions consisting of a dispersion of pigments within the aqueous phase or a previously formed carnauba wax–decyl oleate nanoparticle dispersion, the fraction deposited at the sediment was only referred to as PC_{se} % instead of EE %, because no encapsulation or bonding had occurred.

3.8. Quantification of the carnauba wax

Two 500-mg samples of each nanosuspension were dispersed in 25 mL of an aqueous saccharose solution 20%wt and centrifuged for 1 h at 10,400*g* at room temperature. The equipment used for centrifugation was the same as described in Section 3.4. The supernatant and the sediment were carefully separated with a glass pipette. The excess of saccharose in both fractions was removed applying several successive centrifugation steps. Each step was performed within 10 min at 10,400*g* with addition of 30 mL of double-distilled water. Samples were deposited in 100-mL glass rounded flasks and heated at 90 °C overnight in an oven to eliminate the excess of water and to melt the wax. In order to solubilize the carnauba wax, 45 mL of toluene was added and the obtained solution was heated at 60 °C during 10 min. The carnauba wax solutions were allowed to cool down until room temperature was reached and transferred into 50-mL volumetric flasks. The volumes were finally completed with toluene at room temperature. To eliminate the inorganic pigments, carnauba wax solutions were pre-filtered through special glass microfiber filters GF/B (Whatman Int. Ltd, England) with 47 mm diameter and filtered through 0.2 μm hydrophobic membranes PTFE (Millipore GmbH, Germany) of the same diameter. These two steps were carried out using a Millipore filtration unit. The carnauba wax content was determined at 308 nm using a spectrophotometer Spekol® 1300 (Analytik Jena, Germany). Standard solution containing 50 mg carnauba wax, 50 mg decyl oleate, and 10 mg Tween 80 in 50 mL toluene was prepared and dilutions thereof corresponding to 25, 50, 100, 125, and 150 μg mL^{-1} of carnauba wax were used for calibration purposes. Linearity was obtained with a determination coefficient (R^2) of 0.9983.

4. Results and discussion

4.1. Effect of the temperature on the physical stability of the nanosuspensions

4.1.1. Nanosuspensions of carnauba wax–decyl oleate nanoparticles without pigments

The mean particle size and the polydispersity index of the nanoparticles were selected as reference parameters to evaluate the physical stability of all the nanosuspensions when exposed to three different temperatures, namely 4, 20, and 40 °C, during six months. The particle sizes of the carnauba wax–decyl oleate nanoparticles with a wax–oil ratio of 1:1 were found in a range between 222.04 ± 2.97 and 287.6 ± 29.23 nm with polydispersity indices (PIs) between 0.11 ± 0.04 and 0.20 ± 0.03. These results are depicted in Table 2. Considering the particle sizes observed along this test period, no clear tendencies towards an increase or a reduction of those parameter could be evidenced at any temperature. This statement was supported by the PIs obtained, because narrow distributions in the nanosupensions were kept without further modification. In the case of the wax–oil particles having a wax–oil ratio 2:1, the particle sizes were reported between 263.23 ± 34.12 and 344.17 ± 61.14 nm as shown in Table 2. In comparison to the 1:1 wax–oil particles, a slight tendency to particle size reduction, particularly at 20 °C and at 40 °C, was observed. Here it could be speculated that a small volume contraction occurred spontaneously

Table 2
Effect of the temperatures on the mean particle sizes (MPS) ± SD and polydispersity indices (PI) ± SD of the nanoparticles unloaded and loaded with barium sulfate and strontium carbonate in the lipid phase (LP) at two different wax–oil ratios each

Formulation	Temperature (°C)	Time (days)													
		0		15		30		60		90		120		180	
		MPS (nm)	PI	MPS (nm)	PI	MPS (nm)	PI	MPS (nm)	PI	MPS (nm)	PI	MPS (nm)	PI	MPS (nm)	PI
CW:DO (1:1)	4	246.8 ± 8.25	0.15 ± 0.04	256.9 ± 3.9	0.14 ± 0.04	263.0 ± 17.4	0.15 ± 0.06	252.2 ± 2.7	0.14 ± 0.02	256.6 ± 3.5	0.17 ± 0.02	247.4 ± 6.4	0.12 ± 0.04	265.1 ± 6.4	0.15 ± 0.04
	20			245.9 ± 11.8	0.20 ± 0.04	228.5 ± 10.8	0.13 ± 0.04	225.4 ± 4.7	0.12 ± 0.05	225.4 ± 3.2	0.14 ± 0.03	222.6 ± 5.0	0.12 ± 0.04	251.8 ± 29.3	0.11 ± 0.10
	40			222.0± 2.9	0.11± 0.04	235.0 ± 11.5	0.15 ± 0.04	240.6 ± 7.1	0.13 ± 0.05	275.5 ± 9.3	0.20 ± 0.03	287.6 ± 29.3	0.19 ± 0.05	229.4 ± 8.4	0.14 ± 0.04
CW:DO (2:1)	4	331.6 ± 16.2	0.27 ± 0.01	334.2 ± 61.1	0.37 ± 0.06	300.3 ± 28.6	0.26 ± 0.03	263.2 ± 34.1	0.42 ± 0.14	279.0 ± 22.5	0.32 ± 0.05	272.9 ± 15.5	0.33 ± 0.03	339.8 ± 61.4	0.43 ± 0.06
	20			283.5 ± 14.9	0.33± 0.05	287.5 ± 25.7	0.36 ± 0.05	309.6 ± 47.8	0.40 ± 0.11	290.3 ± 21.4	0.35 ± 0.06	293.5 ± 47.3	0.35 ± 0.09	275.5 ± 11.9	0.42 ± 0.06
	40			288.3 ± 14.3	0.36 ± 0.03	281.9 ± 52.9	0.36 ± 0.10	268.5 ± 27.2	0.35 ± 0.07	300.9 ± 37.8	0.38 ± 0.08	285.7 ± 53.9	0.34 ± 0.10	270.1 ± 11.3	0.40 ± 0.04
CW:DO (1:1)– $BaSO_4$ 2%	4	284.9 ± 19.3	0.25 ± 0.06	262.1 ± 5.3	0.17 ± 0.05	262.7 ± 16.3	0.17 ± 0.05	257.8 ± 6.7	0.16 ± 0.05	270.1 ± 15.6	0.18 ± 0.03	257.2 ± 19.9	0.19 ± 0.05	261.1 ± 3.7	0.15 ± 0.04
	20			269.2 ± 25.9	0.18 ± 0.04	255.6 ± 5.8	0.16 ± 0.04	261.9 ± 4.3	0.16 ± 0.07	285.0 ± 60.5	0.21 ± 0.05	259.6 ± 21.3	0.19 ± 0.05	260.8 ± 4.0	0.18 ± 0.03
	40			262.9 ± 7.8	0.16 ± 0.03	255.4 ± 4.8	0.16 ± 0.03	268.9 ± 23.1	0.19 ± 0.06	305.9 ± 30.9	0.25 ± 0.06	264.8 ± 7.8	0.19 ± 0.04	301.5 ± 8.7	0.19 ± 0.03
CW:DO (2:1)– $BaSO_4$ 6%	4	526.2 ± 39.0	0.37 ± 0.03	477.4 ± 61.8	0.45 ± 0.12	464.5 ± 60.8	0.28 ± 0.05	568.5 ± 121	0.44 ± 0.17	476.4 ± 39.1	0.35 ± 0.07	470.3 ± 54.4	0.39 ± 0.08	545.7 ± 33.9	0.50 ± 0.04
	20			455.8 ± 41.1	0.41 ± 0.09	473.3 ± 92.8	0.50 ± 0.41	481.6 ± 54.1	0.37 ± 0.08	564.1 ± 67.0	0.45 ± 0.10	485.6 ± 49.6	0.41 ± 0.07	555.6 ± 53.8	0.58 ± 0.15
	40			462.8 ± 58.9	0.45 ± 0.18	526.5 ± 56.0	0.50 ± 0.35	549.3 ± 72.4	0.39 ± 0.09	518.6 ± 51.4	0.39 ± 0.05	428.1 ± 28.1	0.36 ± 0.06	571.6 ± 67.7	0.62 ± 0.15
CW:DO (1:1)– $SrCO_3$ 2%	4	261.0 ± 3.4	0.16 ± 0.02	269.1 ± 6.6	0.17 ± 0.05	319.5 ± 48.2	0.23 ± 0.03	310.6 ± 48.2	0.22 ± 0.09	299.8 ± 23.6	0.25 ± 0.06	369.4 ± 44.1	0.30 ± 0.06	395.1 ± 67.0	0.43 ± 0.14
	20			265.6 ± 8.1	0.20 ± 0.05	254.0 ± 16.5	0.18 ± 0.05	271.4 ± 21.8	0.21 ± 0.06	250.8 ± 10.8	0.17 ± 0.03	257.4 ± 6.7	0.21 ± 0.18	267.1 ± 3.8	0.19 ± 0.03
	40			267.8 ± 4.9	0.18 ± 0.04	248.2 ± 5.6	0.18 ± 0.02	257.0 ± 6.4	0.18 ± 0.04	246.6 ± 12.7	0.18 ± 0.02	262.3 ± 16.6	0.18 ± 0.04	264.6 ± 5.3	0.17 ± 0.02
CW:DO (2:1)– $SrCO_3$ 6%	4	438.9 ± 12.9	0.23 ± 0.03	475.2 ± 81.7	0.37 ± 0.12	513.3 ± 38.3	0.38 ± 0.29	585.0 ± 60.0	0.39 ± 0.29	440.1 ± 52.5	0.27 ± 0.04	544.8 ± 64.7	0.40 ± 0.13	537.5 ± 37.6	0.41 ± 0.07
	20			429.8 ± 21.3	0.32 ± 0.03	403.8 ± 17.4	0.36 ± 0.19	452.0 ± 83.0	0.31 ± 0.07	463.0 ± 99.0	0.32 ± 0.06	407.0 ± 35.9	0.29 ± 0.06	425.0 ± 25.5	0.35 ± 0.08
	40			431.2 ± 18.3	0.29 ± 0.03	435.6 ± 14.4	0.32 ± 0.33	480.2 ± 82.9	0.33 ± 0.09	464.8 ± 27.5	0.32 ± 0.06	482.6 ± 22.8	0.34 ± 0.05	494.1 ± 35.3	0.36 ± 0.08

after cooling down and storage in a period of two weeks. Conversely, tendency to size increase was appreciated at 4 °C, particularly after storage of more than 120 days. The PIs for this wax–oil ratio oscillated between 0.26 ± 0.03 and 0.42 ± 0.14.

4.1.2. Nanosuspensions of carnauba wax–decyl oleate matrices loaded with barium sulfate in the lipid phase

At all tested temperatures, the nanoparticles containing barium sulfate with a wax–oil ratio 1:1 showed only minimal variations in their particles sizes as well as in their PIs along the evaluation period. The minimal and maximal particle sizes of this kind of particles were 255.4 ± 4.8 and 301.5 ± 8.7 nm, respectively, whereas the minimal and maximal values for the PIs were 0.15 ± 0.04 and 0.26 ± 0.06 correspondingly. These results are depicted in Table 2. These small variations may be attributed to the good accommodation of the barium sulfate crystals into the wax–oil matrices during the manufacture. Unfortunately this tendency could not be observed in the particles with higher wax–oil load (2:1). In such particles, a wide particle size range varying from 428.1 ± 28.1 to 571.64 ± 67.71 nm was detected. Considering the standard deviations of each point, it was observed that the original particle size of 523.23 ± 38.96 nm at time zero remained at the same level during six months, whereas in terms of their PIs, a wide polydispersity index span ranging from 0.28 ± 0.05 to 0.62 ± 0.15 during the whole evaluation period was detected. According to the results expressed in Table 2, it was not possible to identify clear tendencies to de/aggregation phenomena modifying the particle size at the temperatures applied. Conversely, a tendency towards broad dispersions was signaled in the case of the particles with a wax–oil ratio 2:1 at all temperatures, particularly after 180 days.

4.1.3. Nanosuspensions of carnauba wax–decyl oleate matrices loaded with strontium carbonate in the lipid phase

For those nanosupensions containing strontium carbonate with a wax–oil ratio 1:1, practically no modification of the particle size at the temperatures of 20 and 40 °C could be observed in Table 2. The particle sizes remained between 248.2 ± 5.6 and 271.4 ± 21.8 nm at these temperatures and the PIs were not superior to 0.21 ± 0.06 as depicted in Table 2. On the contrary, a very defined size increase was observed at 4 °C. Particle sizes up to 395.1 ± 67.0 nm were found at this temperature. This increase agreed with the elevated PIs observed after 180 days. The values presented after this point reached 0.43 ± 0.14. On the other hand, when the wax–oil ratio was augmented, a trend to larger particle sizes was more evident at 4 °C. In this case, particle sizes up to 585.0 ± 60.0 nm were detected. At higher temperatures, 20 and 40 °C, such trend towards an increase was not so evident. However, it has to be pointed out that in comparison to the particle size at the time zero (438.9 ± 13 nm), relatively elevated values from 480.2 ± 83 to 494.1 ± 35.3 nm at 40 °C after 60 days might indicate a slight tendency to grow.

4.1.4. Nanosuspensions of carnauba wax–decyl oleate matrices loaded with titanium dioxide in the lipid phase

The nanosuspensions consisting of titanium dioxide in wax–oil (1:1) matrices presented a narrow particle size range between 362.7 ± 38.7 and 428.3 ± 30.5 nm with PIs up to 0.35 ± 0.10 as observed in Table 3. Considering the SD values, these results matched the particle size found at time zero. Consequently, no major changes in this parameter under these conditions could be supposed. On the contrary, using a wax–oil load (2:1), more variability in this parameter was observed. In this case, particles exhibiting mean sizes superior to those at time zero in more than 128 units were found. This was particularly observed at a temperature of 4 °C. In general, the particle sizes having a wax–oil ratio of 2:1 ranged from 534.4 ± 57.8 to 667.3 ± 110.0 nm with corresponding PIs between 0.35 ± 0.20 and 0.68 ± 0.17. Taking into account the particle sizes observed in Table 3, a trend to higher particle sizes was not appreciated. Nevertheless, for the PIs a marked tendency towards size increase could be seen after 15 days. This example showed the usefulness of the PI as co-reference parameter for the long-term physical stability of a nanosuspension.

4.1.5. Carnauba wax–decyl oleate nanoparticles loaded with titanium dioxide (aqueous phase)

To establish differences in particle size stability attributed to the location of the pigment, an alternative manufacturing process to distribute titanium dioxide was carried out by dispersing crystals of this compound in the aqueous phase without encapsulation or agglomeration in the wax–oil matrices. The measurements of the particle size and PI of these nanosuspensions are shown in Table 3. Broadly speaking, the particle sizes of the suspensions prepared using this procedure were smaller than those of the suspensions containing titanium dioxide inside the matrices as observed in Table 3. To explain this fact, it has to be pointed out that by this manufacturing procedure, the formation of lipid nanoparticles bonding internally or enclosing titanium dioxide crystals did not occur, and thus no larger mean particle sizes could be expected [26]. Furthermore, in this case the particle sizes obtained by the measurement technique, i.e., PCS, represented only a mean value of the wax–oil and titanium dioxide nanoparticles dispersed in the aqueous phase as exemplified later in this paper by Fig. 4d. The mean particle sizes of the pigments being encapsulated or bonded by wax–oil matrices at time zero were 403.1 ± 5.91 and 556.2 ± 44.6 nm for the wax–oil loads 1:1 and 2:1 correspondingly, whereas those of the titanium dioxide crystals being distributed in the aqueous phase were 367.6 ± 25.1 and 447.8 ± 24.0 nm in the same order. This demonstrated that the former manufacturing process brought about wax–oil matrices and titanium dioxide crystals in closer contact to each other. Those preparations also exhibited differences attributed to the temperature, since a clear trend towards larger particle sizes at 4 °C independently of the wax–oil ratio was observed after

Table 3
Effect of the temperatures on the mean particle sizes (MPS) ± SD and polydispersity indices (PI) ± SD of the nanoparticles loaded with titanium dioxide either in the lipid phase (LP) or in the aqueous phase (AP) at two different wax–oil ratios each

Formulation	Temperature (°C)	Time (days)															
		0		15		30		60		90		120		180			
		MPS (nm)	PI	MPS (nm)	PI	MPS (nm)	PI	MPS (nm)	PI	MPS (nm)	PI	MPS (nm)	PI	MPS (nm)	PI		
CW:DO (1:1)–TiO_2 2%(LP)	4	403.1 ± 5.9	0.23 ± 0.06	394.8 ± 28.2	0.30 ± 0.08	413.8 ± 19.8	0.28 ± 0.05	389.4 ± 33.1	0.27 ± 0.07	353.6 ± 17.8	0.24 ± 0.03	380.6 ± 12.2	0.23 ± 0.06	384.7 ± 16.4	0.28 ± 0.08		
	20			404.5 ± 26.3	0.33 ± 0.10	378.1 ± 14.2	0.24 ± 0.04	426.5 ± 63.9	0.34 ± 0.13	362.7 ± 38.7	0.28 ± 0.06	396.4 ± 26.3	0.30 ± 0.06	404.9 ± 25.9	0.33 ± 0.07		
	40			406.4 ± 21.2	0.32 ± 0.07	386.7 ± 28.7	0.26 ± 0.08	435.5 ± 105	0.35 ± 0.21	367.4 ± 26.0	0.24 ± 0.03	420.2 ± 31.8	0.32 ± 0.07	428.3 ± 30.5	0.35 ± 0.10		
CW:DO (2:1)–TiO_2 6%(LP)	4	556.2 ± 44.6	0.36 ± 0.19	684.6 ± 104	0.68 ± 0.17	553.0 ± 47.1	0.53 ± 0.35	644.7 ± 97.6	0.52 ± 0.11	555.3 ± 42.8	0.43 ± 0.07	534.4 ± 57.8	0.43 ± 0.09	551.6 ± 60.3	0.53 ± 0.15		
	20			582.0 ± 50.2	0.60 ± 0.14	587.2 ± 137	0.49 ± 0.21	659.8 ± 107	0.54 ± 0.18	636.7 ± 89.7	0.52 ± 0.11	630.3 ± 138	0.56 ± 0.24	596.8 ± 114	0.58 ± 0.16		
	40			565.4 ± 51.2	0.58 ± 0.14	662.9 ± 87.6	0.46 ± 0.08	648.8 ± 148	0.51 ± 0.17	667.3 ± 110	0.59 ± 0.17	596.0 ± 125	0.51 ± 0.18	623.1 ± 102	0.66 ± 0.19		
CW:DO (1:1)–TiO_2 2% (AP)	4	367.6 ± 25.1	0.24 ± 0.03	486.5 ± 62.1	0.35 ± 0.07	493.5 ± 37.2	0.41 ± 0.11	554.5 ± 112	0.53 ± 0.15	578.9 ± 31.6	0.38 ± 0.10	453.4 ± 111	0.33 ± 0.17	553.6 ± 59.5	0.31 ± 0.08		
	20			327.9 ± 12.0	0.20 ± 0.03	333.5 ± 24.1	0.26 ± 0.04	328.6 ± 21.4	0.26 ± 0.06	334.2 ± 17.8	0.23 ± 0.08	364.7 ± 38.7	0.27 ± 0.06	337.8 ± 21.9	0.27 ± 0.09		
	40			326.3 ± 12.8	0.22 ± 0.03	325.8 ± 27.5	0.27 ± 0.04	340.9 ± 17.8	0.28 ± 0.08	348.9 ± 23.8	0.26 ± 0.10	380.9 ± 46.7	0.30 ± 0.07	325.4 ± 46.7	0.24 ± 0.03		
CW:DO (2:1)–TiO_2 6%(AP)	4	447.7 ± 24.0	0.23 ± 0.06	535.9 ± 88.3	0.31 ± 0.07	495.3 ± 134	0.35 ± 0.09	587.2 ± 45	0.43 ± 0.08	615.9 ± 64.5	0.36 ± 0.10	491.1 ± 105	0.32 ± 0.07	600.9 ± 41.6	0.46 ± 0.08		
	20			407.6 ± 35.7	0.29 ± 0.12	417.1 ± 40.7	0.29 ± 0.12	401.8 ± 26.7	0.37 ± 0.17	412.4 ± 14.8	0.27 ± 0.05	388.2 ± 21.4	0.25 ± 0.06	412.1 ± 20.7	0.33 ± 0.08		
	40			380.9 ± 11.4	0.26 ± 0.03	397.7 ± 19.5	0.27 ± 0.06	406.0 ± 35.2	0.36 ± 0.10	404.7 ± 48.5	0.31 ± 0.11	390.6 ± 26.1	0.24 ± 0.06	411.9 ± 24.3	0.34 ± 0.09		

15 days. At this temperature, the particle sizes oscillated between 486.5 ± 62.1 and 535.9 ± 88.3 nm. In contrast to this evident change, it could be observed that the particle sizes of the nanosuspensions stored at 20 and 40 °C remained practically without change. The particle sizes obtained for the wax–oil ratio 1:1 ranged from 367.6 ± 25.1 to 380.0 ± 46.7 nm and that of the particles with a wax–oil ratio 2:1 varied between 380.8 ± 11.36 and 417.08 ± 40.74 nm. These differences resulted only from the wax–oil ratio and not because of the temperature within the whole period of observation. The PIs also registered a trend towards increased particle sizes at 4 °C for both wax–oil ratios used after 15 days, being easily recognized after 60 days. At this temperature, the PI values were shown between 0.31 ± 0.08 and 0.53 ± 0.14 for the lowest wax–oil ratio, meanwhile those of the highest wax–oil ratio were found between 0.31 ± 0.06 and 0.46 ± 0.08. On the whole, higher PIs were found when the temperature was close to 0 °C independently of the wax load.

4.2. The effect of the wax–oil ratio and the amount of pigment load on the physical stability of the nanosuspensions

Considering the aforementioned results (Section 4.1.1–4.1.5) it could be observed that the particle sizes of the nanosuspensions evaluated showed only minor changes when stored at 20 and at 40 °C during six months. These observations coincided with the information derived from the zeta potential measurements of a former study [26]. According to this, those particles showing zeta potentials $\leqslant -21$ mV, i.e., pigment-free wax–oil matrices and pigment-loaded wax–oil matrices, were not expected to form agglomerates at room temperature for long time [29]. Conversely, a trend to destabilization of most of the nanosuspensions, identified by a particle size increase and variable broad distributions (PI > 0.25) [30], occurred at 4 °C even after 15 days of start of the evaluation in some cases (Section 4.1.5). It has to be noticed that the latter phenomenon was particularly accentuated in those nanosuspensions having higher wax–oil ratios [26]. According to this, the variability in particle size and polydispersity was related with the wax–oil ratios used and the amount of the inorganic crystal loads. Therefore, the nanosuspensions having lower wax–oil ratios combined with lower pigment loads showed less variation of particle size and polydispersity than that of the nanosuspensions containing high wax–oil ratios accompanied by high pigment loads. The possible explanation lies on a better resistance of the smaller particles to the mechanical stress exerted by the osmotic forces, as stated by Talsma et al. [31] in the case of liposomes. On the other hand, the particle size increase observed could be justified by the particle aggregation phenomena, i.e., homogeneous or heterogeneous particle associations between pigment crystals and wax–oil matrices, and eventually by a nucleation of wax crystals occurring preferential at near to zero and subzero temperatures. Apparently, for the nanosupensions here exposed, the association between inorganic crystals especially observed in the case of titanium dioxide, being dispersed in wax–oil nanosuspensions without capsule formation at 4 °C (Table 3), seemed to be more favored than that between lipid nanoparticle and inorganic pigment crystal or between nanoparticles themselves. This argument could be supported in virtue of the slight modifications of the particle size at the same temperature undergone by the wax–oil particles without pigment load (Table 2). Furthermore, it has to be signaled that, in previous studies, the titanium dioxide dispersions without wax–oil matrices possessed very low zeta potentials (ca. −6 mV), which indicated an intrinsic tendency to built agglomerates [29]. The particle size and PI measurements exposed here were performed at room temperature, but, as observed, a spontaneous deagglomeration did not take place. The aforementioned phenomena seem not to be exclusive of these nanosupensions, because other colloids such as liposomes or solid lipid nanoparticles have demonstrated to exhibit particle size increase at near to zero and subzero temperatures [32] and in order to avoid the troubles thereof, the use of cryoprotectants in colloidal systems as part of the formulation has been introduced in the past, e.g., trehalose and other carbohydrates for liposome protection [33,34].

Another strategy to keep the original mean particle size of the nanoparticles could be their incorporation into creams or gels as demonstrated by Lippacher et al. [35] in the case of SLN. Other factors to the stability of those systems are the effect of the surfactant and its concentration and the effect of the antifoamer used in the formulation in virtue of the contribution of those substances to the superficial repulsion forces of the particles in the nanosuspension [36]. However, these variables were not included during this study.

4.3. Centrifugation and TEM visualization of the nanosuspensions

As a result of the 1-h centrifugation tests performed using samples of different nanosuspensions, three major fractions denominated could be identified in all the assays. To illustrate this, the drawing in Fig. 1 is presented.

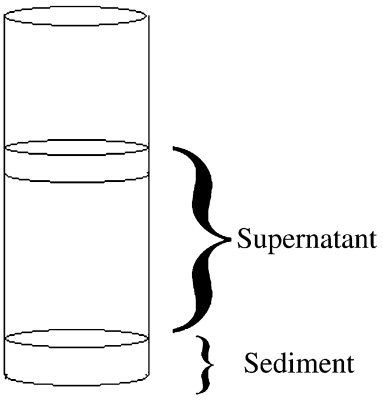

Fig. 1. Typical separation of the nanosuspensions after centrifugation, in which the supernatant is divided in two fractions.

As depicted here, apart from the sediment, there are two well-defined fractions at the middle and the upper part of the tubes constituting the supernatant. Samples from those fractions were removed and freeze fractured for TEM viewing as indicated in Section 3.5. The structures found in the upper part of the supernatant are shown in Figs. 2a–d. In this fraction, only pigment-free nanoparticles were observed, in other words, only the wax–oil matrices not participating in the encapsulation, bonding or attachment of inorganic pigments. The similarities between those particles could be easily recognized, since round particles showing in some cases lamellar structures at their borders were identified in all samples [37]. In contrast to this parallelism, the middle fraction showed different structures in all the cases. Accordingly, Fig. 3a presented non-deagglomerated barium sulfate crystals probably being attached to the surface of the wax–oil matrices. This sporadic association certainly changed sedimentation behavior of the wax–oil matrices. In Fig. 3b, isolated agglomerates of strontium carbonate crystals were scarcely found, whereas in the case of titanium dioxide (Fig. 3c), agglomerated crystals being encapsulated by oil droplets apparently derived from the decyl oleate were observed. This means that during the homogenization process, some titanium dioxide crystals were expelled from the matrix and in virtue of their lipophobic coating, an entrapment inside decyl oleate droplets

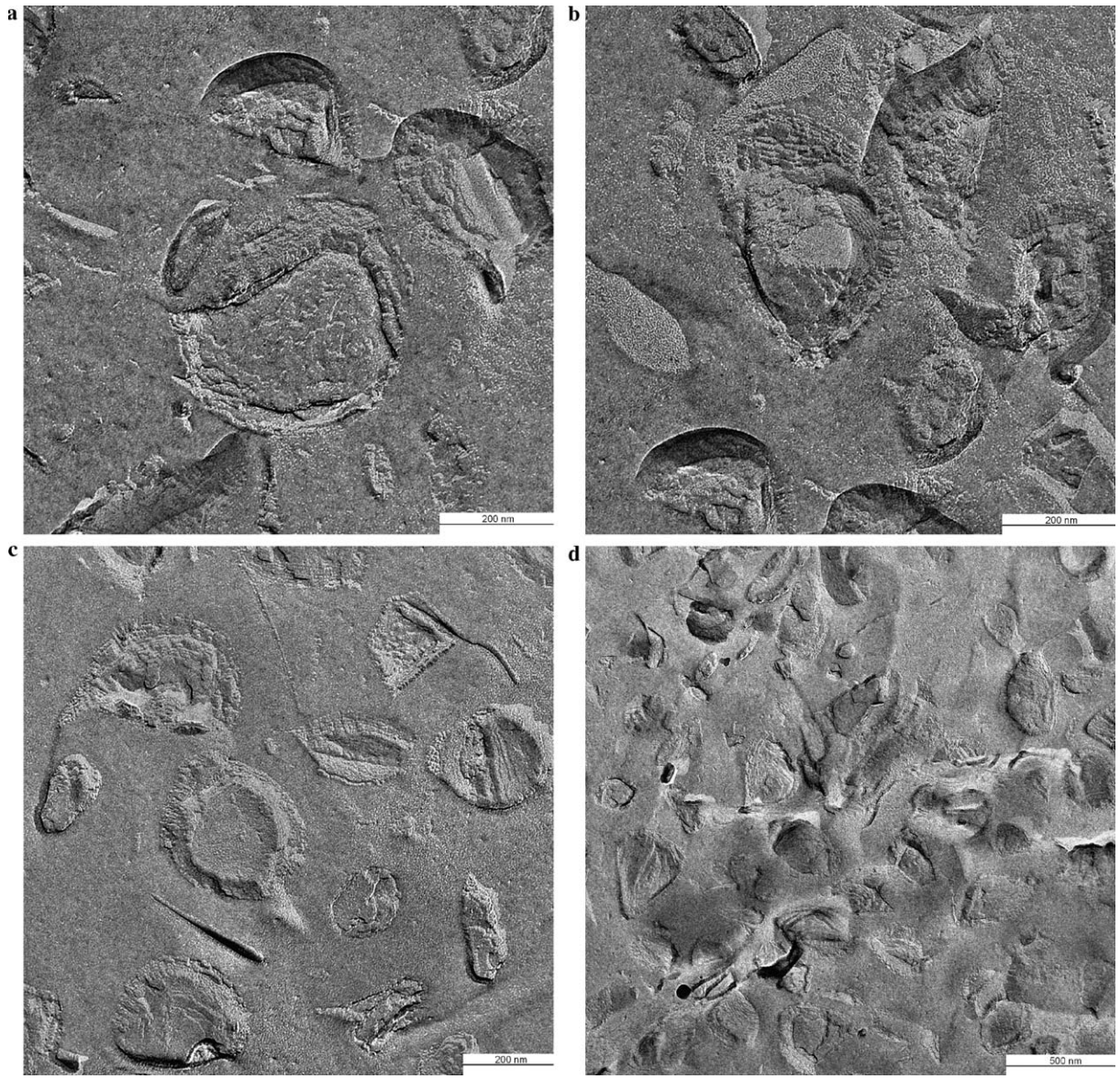

Fig. 2. (a) TEM of a freeze fractured sample of the upper part of the supernatant of a preparation containing barium sulfate crystals (4%wt) being encapsulated by carnauba wax–decyl oleate (2:1) nanoparticles. (b) TEM of a freeze fractured sample of the upper part of the supernatant of a preparation containing strontium carbonate crystals (4%wt) being encapsulated by carnauba wax–decyl oleate (2:1) nanoparticles. (c) TEM of a freeze fractured sample of the upper part of the supernatant of a preparation containing titanium dioxide crystals (6%wt) being encapsulated by carnauba wax–decyl oleate (2:1) nanoparticles. (d) TEM of a freeze fractured sample of the upper part of the supernatant of a preparation containing titanium dioxide crystals (6%wt) dispersed in carnauba wax–decyl oleate (2:1) nanoparticles.

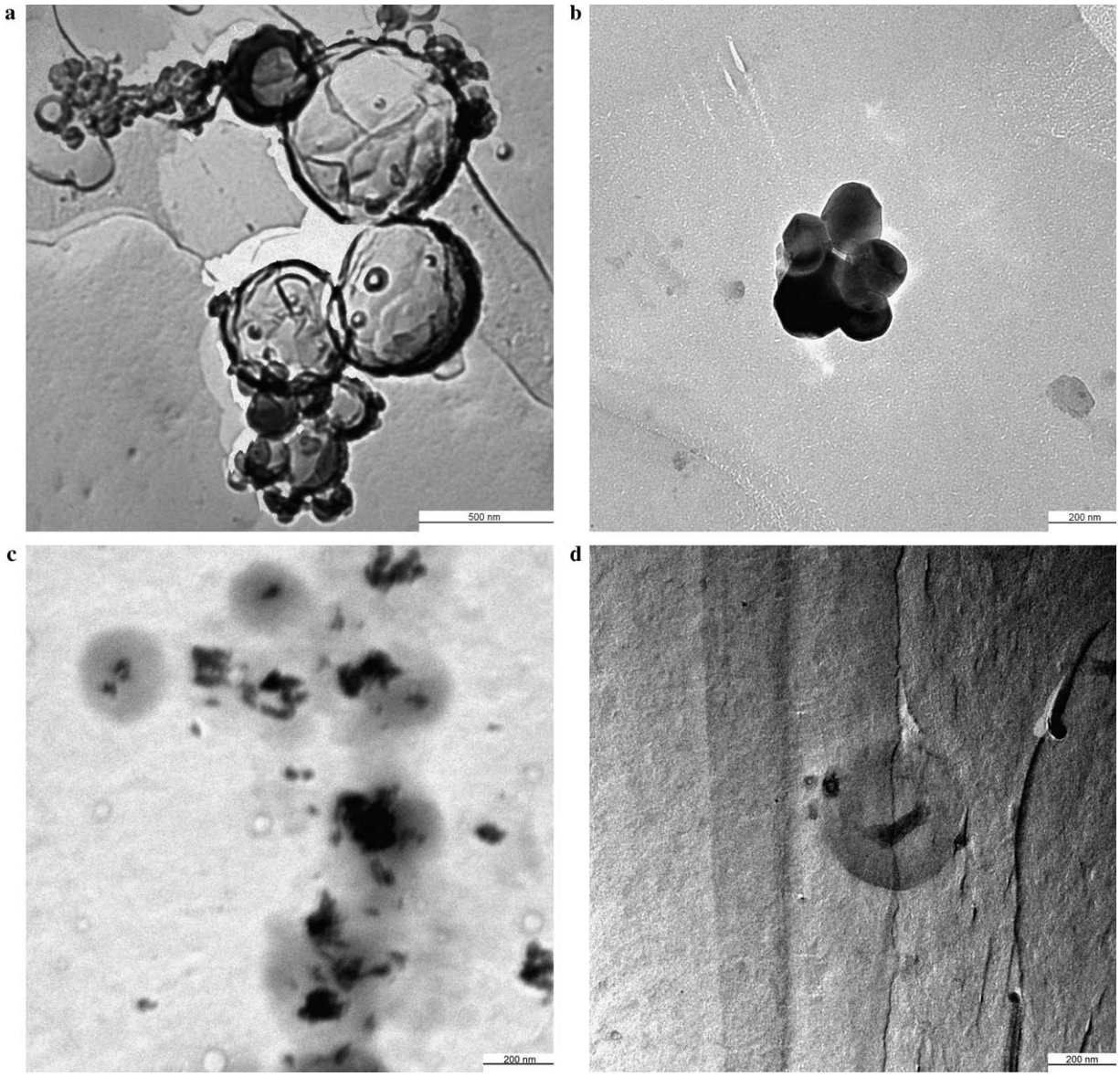

Fig. 3. (a) TEM of a freeze fractured sample of the bottom part of the supernatant of a preparation containing barium sulfate crystals (4%wt) being encapsulated by carnauba wax–decyl oleate (2:1) nanoparticles. (b) TEM of a freeze fractured sample of the bottom part of the supernatant of a preparation containing strontium carbonate crystals (4%wt) being encapsulated by carnauba wax– decyl oleate (2:1) nanoparticles. (c) TEM of a freeze fractured sample of the bottom part of the supernatant of a preparation containing titanium dioxide crystals (6%wt) being encapsulated by carnauba wax–decyl oleate (2:1) nanoparticles. (d) TEM of a freeze fractured sample of the bottom part of the supernatant of a preparation containing titanium dioxide crystals (6%wt) dispersed in carnauba wax–decyl oleate (2:1) nanoparticles.

took place. The same phenomenon at a very less extension was observed when the titanium dioxide crystals were distributed in a wax–oil matrix dispersion as seen in Fig. 3d. In similar way to the views presented in the middle part of the centrifugates, diverse structures were also seen at the sediment. Fig. 4a shows an accumulation of wax–oil nanoparticles containing barium sulfate. In this figure, well-defined spheres were observed and it was important to point out that no free barium sulfate crystals were found, which could be attributed to their encapsulation inside the wax–oil matrices. This observation has been previously described in other works [6]. In Fig. 4b, the encapsulation of strontium carbonate crystals can be visualized. In contrast to Fig. 4a, the strontium carbonate crystals were not fully covered by the wax–oil matrix, consequently they could be identified as black spots over the lipid matrices and some of them could also be found at the borders. In reference to the sediment of the nanosuspensions containing wax–oil matrices loaded with titanium dioxide, structures demonstrating the encapsulation of those crystals were localized as depicted in Fig. 4c. In this figure, the contrast of the dark titanium dioxide needles forming agglomerates with a clear medium being delimited by the lipid matter can be seen. Contrarywise, when the pigments were only dispersed in the aqueous phase, no entrapment occurred as illustrated in Fig. 4d. In spite of this, wax–oil

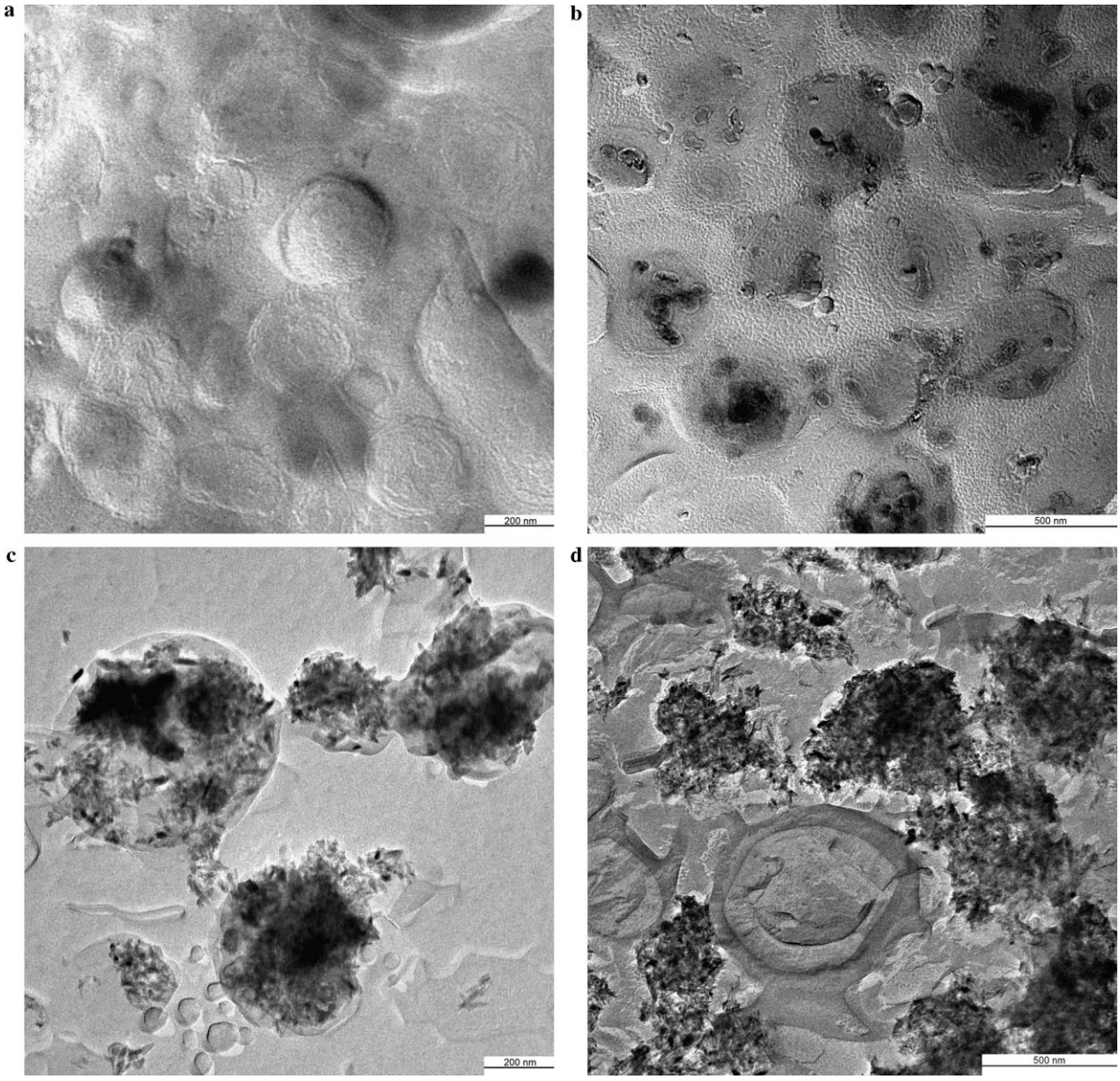

Fig. 4. (a) TEM of a freeze fractured sample of the sediment of a preparation containing barium sulfate crystals (4%wt) being encapsulated by carnauba wax–decyl oleate (2:1) nanoparticles. (b) TEM of a freeze fractured sample of the sediment of a preparation containing strontium carbonate crystals (4%wt) being encapsulated by carnauba wax–decyl oleate (2:1) nanoparticles. (c) TEM of a freeze fractured sample of the sediment of a preparation containing titanium dioxide crystals (6%wt) being encapsulated by carnauba wax–decyl oleate (2:1) nanoparticles. (d) TEM of a freeze fractured sample of the sediment of a preparation containing titanium dioxide crystals (6%wt) dispersed in carnauba wax–decyl oleate (2:1) nanoparticles.

matrices were also detected at the sediment as observed in the lower middle part of this figure, which could be probably explained by the surface association between titanium dioxide and the wax–oil matrices changing the density of the latter.

4.4. Distribution of pigment content in the centrifuged samples of those nanosuspensions based on pigments dispersed in molten wax–oil mixtures

As described in Section 3.5 the fraction of the nanosuspensions located at the supernatant (PC_{su} %) represented the fraction of the pigment content being not encapsulated or bonded by wax–oil matrices of a nanosuspension, whereas that located at the sediment (PC_{se} %) represented those inorganic crystals conforming part of the internal structure of the wax–oil matrices. Therefore, the PC_{se} % was labeled as the entrapment efficiency EE% of nanosuspensions, which reflects the efficiency of the process to incorporate pigments into wax–oil matrices in terms of the pigment load used for the nanosuspensions prepared by incorporating the pigment into a molten wax–oil mixture. This argument could be confirmed considering the views exposed in Figs. 4a–c. The sum of pigment at the supernatant (PC_{su} %) and that at the sediment (PC_{se} %) referred to as the total content of pigment (PC_t %) and the EE% are shown in Table 4. As seen in this table, the PC_t % computed matched most of the theoretical values

Table 4
The total content of pigment (%) ± SD and the entrapment efficiency (EE%) ± SD of the nanosuspensions containing wax–oil matrices loaded with pigments dispersed in the lipid phase

Pigment	Total pigment content (%)				
	Theoretical values	Experimental values Wax–oil ratio		Entrapment efficiency (EE%) Wax–oil ratio	
		(1:1)	(2:1)	(1:1)	(2:1)
$BaSO_4$	2	2.00 ± 0.34	1.91 ± 0.24	95.73 ± 2.27	88.60 ± 2.47
	4	3.81 ± 0.26	4.30 ± 0.15	97.56 ± 2.42	97.91 ± 1.76
	6	5.60 ± 0.12	6.08 ± 0.08	97.99 ± 1.36	91.96 ± 0.67
$SrCO_3$	2	1.64 ± 0.04	1.80 ± 0.17	87.08 ± 8.87	90.14 ± 6.04
	4	4.38 ± 0.21	3.99 ± 0.23	93.04 ± 7.21	94.84 ± 4.93
	6	5.45 ± 0.32	5.67 ± 0.13	88.48 ± 7.42	94.50 ± 1.64
TiO_2(LP)	2	1.70 ± 0.06	2.20 ± 0.24	85.52 ± 3.28	94.65 ± 1.84
	4	3.50 ± 0.18	3.75 ± 0.24	90.31 ± 2.99	88.38 ± 8.39
	6	5.97 ± 0.51	5.86 ± 0.45	97.06 ± 0.62	97.53 ± 0.97

LP, lipid phase.

of pigment content in all the nanosuspensions meanwhile, the EE% of those nanosupensions oscillated between 85.52% ± 3.28% and 97.99% ± 1.36%. According to the Table 4, barium sulfate presented EEs% ranging from 88.60% ± 2.47% to 97.99% ± 1.36%; strontium carbonate exhibited EEs% between 87.08% ± 8.87% and 94.50% ± 1.64% and titanium dioxide reported EE% values between 85.52% ± 3.28% and 97.53% ± 0.97%. Particular modifications of the EE% in respect of the type of pigment, the pigment concentration, and the wax–oil ratio applied for the entrapment could not be clearly differentiated and the variation presented in the table was attributed to the sample handling. On the other hand, the EE% values under 100% agreed with the localization of the inorganic crystals in the supernatant (PC_{su} %), particularly at the lower part of it, as observed in Figs. 3a–d. Those values were not depicted in Table 4.

4.5. Distribution of titanium dioxide in the centrifuged samples of those nanosuspensions based on titanium dioxide crystals distributed in the aqueous phase of wax–oil matrices dispersions

Table 5 shows the expected and the experimental values of the titanium dioxide content in the nanosuspensions and those of the PC_{se} % as well. As stated in Section 3.7, PC_{se}% did not represent the EE% for this kind of nanosuspensions. In Table 5 it was seen that the total pigment content found (PC_t %) agreed with the expected values meanwhile, the PC_{se} % values observed were very high ($\geqslant$98.09%). According to these results, it can be stated that most of the pigment was found at the sediment after being centrifuged and only less than 2% of it was found at the supernatant. The high concentration of the titanium dioxide at the sediment is appreciated in Fig. 4d. In this figure, it was important to notice that some wax–oil matrices were also seen at the sediment. The possible explanation resides in the high pressure homogenization process allowing the attachment of some pigment crystals to the wax–oil matrices, by which their density was modified so that they could settle along with the rest of pigment after centrifugation.

4.6. Distribution of carnauba wax in the centrifuged samples of the nanosuspensions

The carnauba wax found at the sediment represented the fraction encapsulating, bonding or attaching inorganic sunscreens depending on the process used for the manufacture of nanosuspensions, whereas the fraction at the supernatant represented the pigment-free fraction or the fraction

Table 5
The total content of pigment (%) ± SD and the entrapment efficiency (EE%) ± SD of the nanosuspensions containing wax–oil matrices loaded with titanium dioxide dispersed in the aqueous phase

Pigment	Total pigment content (%)				
	Theoretical values	Experimental values Wax–oil ratio		PC_{se} % Wax–oil ratio	
		(1:1)	(2:1)	(1:1)	(2:1)
TiO_2 (AP)	2	1.88 ± 0.21	1.74 ± 0.05	98.88 ± 0.32	98.09 ± 0.39
	4	3.61 ± 0.25	3.69 ± 0.09	98.21 ± 1.67	99.14 ± 1.22
	6	5.89 ± 0.47	5.64 ± 0.04	98.77 ± 0.82	99.73 ± 0.37

PC_{se} %, pigment content at the sediment; AP, aqueous phase.

Table 6
The distribution of carnauba wax (%) at the supernatant and at the sediment of the centrifuged samples of the nanosuspensions containing pigments

Pigment	Total pigment content (%)	Carnauba wax content (%)			
		Wax–oil ratio (1:1)		Wax–oil ratio (2:1)	
		Supernatant	Sediment	Supernatant	Sediment
$BaSO_4$	2	46.4	53.6	42.0	58.0
	4	35.3	64.7	32.0	67.0
	6	33.6	66.4	29.2	70.8
$SrCO_3$	2	39.6	60.4	33.1	66.9
	4	33.2	66.8	31.7	68.3
	6	27.7	72.3	27.9	72.1
TiO_2(LP)	2	29.1	70.9	24.9	75.1
	4	26.2	73.9	21.5	78.5
	6	24.3	75.7	18.8	81.2
TiO_2(AP)	2	77.0	23.0	75.1	24.9
	4	74.4	25.6	71.3	28.7
	6	73.8	26.2	64.6	35.4

LP, lipid phase; AP, aqueous phase.
The content of carnauba wax in the supernatant fraction of those nanosuspensions containing no pigments was equal to 100%.

with minor surface contact with pigment. This could be illustrated by Figs. 2a, 3, and 4d. The results of the carnauba wax distribution after centrifugation are shown in Table 6. In general, it can be observed that more carnauba wax was found at the sediment when higher loads of it were used. Amongst pigments, titanium dioxide seemed to exhibit more affinity to carnauba wax, since higher values of wax content were found when titanium dioxide was used and these values oscillated between 70% and 81.2%. For barium sulfate, the wax content at the sediment varied between 53.6% and 70.8%, meanwhile strontium carbonate showed wax contents at the sediment between 60.4% and 72.1%. Differences in the contact between wax and pigment could be attributed to the lipophilic character of the pigments [24], particularly in the case of titanium dioxide, since this pigment possessed a lipophilic coating. Other properties probably exhibiting an effect were the primary particle size, the density of the pigments, the porosity, the trend to form agglomerates and the surface area of the pigments. However, those effects were not evaluated in this study. In the case of the titanium dioxide dispersed in the aqueous phase, it was observed that between 23% and 35.4% of the carnauba wax used was found at the sediment, which indicated that the density of these particles was modified by the pigment being incrusted onto the wax matrices during the homogenization process.

5. Conclusions

Nanosuspensions based on carnauba wax–decyl oleate matrices containing inorganic pigments could be stored during six months at 20 and at 40 °C inside chromatographic brown bottles sealed with butyl/PTFE rubber stoppers without observing elevated variability in their mean particle size and polydispersity. However, the storage at 4 °C favored the increase of the particle sizes and altered the homogeneity of the preparations. This tendency was particularly observed when high loads of carnauba wax were used and when the pigment was not incorporated inside the lipid matrices. To avoid these instability phenomena, either the use of formulations containing cryoprotectants or the incorporation of the nanoparticles into creams or hydrogels directly after production is suggested for further formulations. On the whole, it can be stated that wax–oil matrices with lower pigment loads were thermodynamically more stable than those with higher pigment loads. On the other hand, the presence of different particles constituting the nanosuspensions was demonstrated by the centrifugation tests. Hence, wax–oil matrices without inorganic pigment; decyl oleate droplets with inorganic pigments; wax–oil matrices loaded inside with pigments and inorganic pigments attached to the surface of wax–oil matrices were the species mainly reported. The results of the encapsulation efficiency showed that most of the pigment content could be encapsulated or bonded by wax–oil matrices. However, it was also evident that not all the carnauba wax used participated in the encapsulation or attachment of the pigments.

Acknowledgements

Mr. Villalobos is recipient of a fellowship granted by the Deutscher Akademischer Austauschdienst (DAAD). The availability of the TEM at the Institute of Physics of the Condensed Matter of the Technical University of Braunschweig and the technical assistance of Mr. Hanno Dierke are gratefully acknowledged. Solvay GmbH, Kemira Chemicals GmbH, and Brenntag GmbH are thanked for the donation of substances.

References

[1] R.H. Müller, M. Radtke, S. Wissing, Solid lipid nanoparticles (SLN) and nanostructured lipid carriers (NLC) in cosmetic and dermatological preparations, Adv. Drug Deliv. Rev. 54 (2002) S131–S155.
[2] V. Jenning, K. Mäder, S. Gohla, Solid lipid nanoparticles (SLN™) based on binary mixtures of liquid and solid lipids: a ^{1}H NMR study, Int. J. Pharm. 205 (2000) 15–21.
[3] W. Mehnert, K. Mäder, Solid lipid nanoparticles. Production, characterization and applications, Adv. Drug Deliv. Rev. 47 (2001) 165–196.
[4] A. Saupe, S.A. Wissing, A. Lenk, C. Schmidt, R.H. Müller, Solid lipid nanoparticles (SLN) and nanostructured lipid carriers (NLC) – structural investigations on two different carrier systems, Bio-Med. Mat. Eng. 15 (2005) 393–402.
[5] R.H. Müller, M. Radtke, S.A. Wissing, Nanostructured lipid matrices for improved microencapsulation of drugs, Int. J. Pharm. 242 (2002) 121–128.
[6] J. R. Villalobos-Hernández, C. C. Müller-Goymann, Evaluation of a novel nanoparticulate carrier system for inorganic sunscreens based on carnauba wax and decyl oleate, in: Proceedings of the International Meeting on Pharmaceutics, Biopharmaceuticals, and Pharmaceutical Technology, Nuerenberg, March 2004, pp. 487–488.
[7] W. Grimm, Basic principles of stability testing, in: W. Grimm, K. Krummen (Eds.), Stability Testing in the EC, Japan and the USA,

Wissenschaftliche Verlagsgesellschaft mbH, Stuttgart, Germany, 1984, pp. 189–204.
[8] N. Weiner, Introduction, in: H.A. Liebermann, M.M Rieger, S. Banker (Eds.), Pharmaceutical Dosage Forms: Disperse Systems, vol. 1, Marcel Dekker, New York, NY, 1996, pp. 1–14.
[9] P.H. Stahl, Basic principles of stability testing, in: W. Grimm, K. Krummen (Eds.), Stability Testing in the EC, Japan and the USA, Wissenschaftliche Verlagsgesellschaft mbH, Stuttgart, Germany, 1984, pp. 45–65.
[10] A.K. Reng, Stabilitätsprüfungen von dispersen Zubereitungen, in: Asche, D. Essig, C. Schmidt (Eds.), Technologie von Salben, Suspensionen und Emulsionen, Wissenschaftliche Verlagsgesellschaft mbH, Stuttgart, Germany, 1984, pp. 189–204.
[11] R. Nash, Pharmaceutical suspensions, in: H.A. Liebermann, M.M Rieger, S. Banker (Eds.), Pharmaceutical Dosage Forms: Disperse Systems, vol. 2, Marcel Dekker, New York, NY, 1996, pp. 1–46.
[12] M.J. Falkiewicz, Theory of suspensions, in: H.A. Liebermann, M.M Rieger, S. Banker (Eds.), Pharmaceutical Dosage Forms: Disperse Systems, vol. 1, Marcel Dekker, New York, NY, 1996, pp. 32–41.
[13] W. Grimm, General concept of stability testing, in: W. Grimm, K. Krummen (Eds.), Stability Testing in the EC, Japan and the USA, Wissenschaftliche Verlagsgesellschaft mbH, Stuttgart, Germany, 1984, pp. 191–223.
[14] M.I.R.M. Santoro, D. Almança Gonçalves Da Costa, E. Oliveira, E.R.M. Kedor-Hackmann, A.K. Singh, The effect of packaging materials on the stability of sunscreen emulsions, Int. J. Pharm. 297 (2005) 197–203.
[15] H.N. Bhargava, D.W. Nicolai, B.J. Oza, Topical suspensions, in: H.A. Liebermann, M.M Rieger, S. Banker (Eds.), Pharmaceutical Dosage Forms: Disperse Systems, vol. 2, Marcel Dekker, New York, NY, 1996, pp. 183–242.
[16] R.H. Müller, K. Mäder, S. Gohla, Solid lipid nanoparticles for controlled delivery – a review of the state of art, Eur. J. Pharm. Biopharm. 50 (2000) 161–177.
[17] K. Westesen, H. Bunjes, M.H.J. Koch, Physicochemical characterization of lipid nanoparticles and evaluation of their drug loading capacity and sustained release potential, J. Control Release 48 (1997) 223–236.
[18] R.H. Müller, K. Mäder, S. Gohla, Solid lipid nanoparticles (SLN) for controlled drug delivery – a review of the state of art, Eur. J. Pharm. Biopharm. 50 (2000) 161–167.
[19] S.A. Wissing, O. Kayser, R.H. Müller, Solid lipid nanoparticles for parenteral drug delivery, Adv. Drug Deliv. Rev. 56 (2004) 1257–1272.
[20] C. Freitas, R.H. Müller, Correlation between long-term stability of solid lipid nanoparticles (SLN™) and crystallinity of the lipid phase, Eur. J. Pharm. Biopharm. 47 (1999) 125–132.
[21] S. Lim, C. Kim, Formulation parameters determining the physicochemical characteristics of solid lipid nanoparticles loaded with all-trans retinoic acid, Int. J. Pharm. 234 (2002) 135–146.
[22] M.M. Jiménez, J. Pelletier, M.F. Bobin, M.C. Martini, Influence of encapsulation on the in vitro percutaneous absorption of octyl methoxycinnamate, Int. J. Pharm. 272 (2004) 45–55.
[23] H. Marchais, S. Benali, J.M. Irache, C. Tharasse-Bloch, O. Lafont, A.M. Orecchioni, Entrapment efficiency and initial release of phenylbutazone from nanocapsules prepared from different polyesters, Drug Dev. Ind. Pharm. 24 (9) (1998) 833–888.
[24] F. Tiarks, K. Landfester, M. Antonietti, Encapsulation of carbon black by miniemulsion polymerisation, Macromol. Chem. Phys. 202 (2001) 51–60.
[25] K. Jores, W. Mehnert, M. Drechsler, H. Bunjes, C. Johann, K. Mäder, Investigations on the structure of solid lipid nanoparticles by photon correlation spectroscopy, field-flow fractionation and transmission electron microscopy, J. Control Release 95 (2004) 217–227.
[26] J.R. Villalobos-Hernández, C.C. Müller-Goymann, Novel nanoparticulate carrier systems based on carnauba wax an decyl oleate for the dispersion of inorganic sunscreens in aqueous media, Eur. J. Pharm. Biopharm. 60 (2005) 113–122.
[27] R.H. Müller, B.H.L. Böhm, Dispersion techniques for laboratory and industrial scale processing, Wissenschaftliche Verlagsgesellschaft mbH Stuttgart (2001) 16–29.
[28] X.Y. Cheng, J.X. Liang, Q.G. Li, Construction of RNA-containing virus-like nanoparticles expression vector with cysteine residues on surface and fluorescent decoration, Yi Chuang Xue Bao 32 (2005) 874–878.
[29] R.H. Müller, Zetapotential und Partikelladung in der Laborpraxis, Wissenschaftliche Verlagsgesellschaft mbH Stuttgart (1996) 52–53.
[30] R.H. Müller, R. Schuhmann, Teilchengrößenmessung in der Laborpraxis, Wissenschaftliche Verlagsgesellschaft mbH Stuttgart (1996) 23–30.
[31] H. Talsma, M.J. van Steenbergen, D.J.A. Crommelin, The cryoprotection of liposomes 2. Effect of the particle size on the crytallization behavior and marker retention, Cryobiology 29 (1992) 80–86.
[32] E.B. Souto, S.A. Wissing, C.M. Barbosa, R.H. Müller, Development of a controlled release formulation based on SLN and NLC for topical clotrimazole delivery, Int. J. Pharm. 278 (2004) 71–77.
[33] L.M. Crowe, J.H. Crowe, A. Rudolph, C. Wormersley, L. Appel, Preservation of freeze-dried liposomes by trehalose, Arch. Biochem. Biophys. Acta 242 (1985) 240–247.
[34] L.M. Crowe, C. Wormersley, J.H. Crowe, D. Reid, L. Appel, A. Rudolph, prevention of fusion and leakage in freeze-dried liposomes by carbohydrations, Arch. Biochem. Biophys. Acta 861 (1986) 131–140.
[35] A. Lippacher, R.H. Müller, K. Mäder, Liquid and semisolid SLN™ dispersions for topical application: rheological characterization, Eur. J. Pharm. Biopharm. 58 (2004) 561–567.
[36] S. de Chasteignier, G. Cavé, H. Fessi, J.P. Devissaguet, F. Puisieux, Freeze-Drying of itraconazole-loaded nanosphere suspensions: a feasibility study, Drug Dev. Res. 38 (1996) 116–124.
[37] C.C. Müller-Goymann, Physicochemical characterization of colloidal drug delivery systems such as reverse micelles, vesicles, liquid crystals and nanoparticles for topical administration, Eur. J. Pharm. Biopharm. 58 (2004) 343–356.